

## Article

# Initial Occurrence State and Movability Evaluation of the Gulong Shale Oil Reservoir, Songliao Basin

Guozhong Zhao <sup>1,2</sup>, Linsong Cheng <sup>3</sup>, Pin Jia <sup>3</sup>, Yong Liu <sup>1,2</sup>, Haoran Feng <sup>3,\*</sup>, Tie Kuang <sup>1,2</sup> and Qingzhen Wang <sup>1,2</sup>

<sup>1</sup> Exploration and Development Research Institute of Daqing Oilfield Company Ltd., Daqing 163712, China; zhaoguozh@petrochina.com.cn (G.Z.); swpiliuyong@petrochina.com.cn (Y.L.); kuangtie@petrochina.com.cn (T.K.); wangqingzhen@petrochina.com.cn (Q.W.)

<sup>2</sup> Heilongjiang Provincial Key Laboratory of Reservoir Physics & Fluid Mechanics in Porous Medium, Daqing 163712, China

<sup>3</sup> School of Petroleum Engineering, China University of Petroleum (Beijing), Beijing 102249, China; lscheng@cup.edu.cn (L.C.); pjia@cup.edu.cn (P.J.)

\* Correspondence: 2022210271@student.cup.edu.cn; Tel.: +86-156-1180-3071

**Abstract:** The Qing-1 layer of the Gulong Depression in the northern Songliao Basin is a liquid-rich shale oil reservoir that has the characteristics of nanopores, high maturity, high gas/oil ratio (GOR), etc. The production performance of wells in the Gulong shale oil reservoir shows the characteristics of “single gas production followed by oil-gas production”. It is difficult to analyze the initial occurrence state and movability of fluid in the shale nanopores using conventional methods. In this study, a comprehensive method, including phase behavior analysis, physical experiments, and molecular simulation, was established to analyze the initial occurrence state and movability of fluid in the Gulong shale oil reservoir. The phase state of the fluid was calculated by the equation of state (EOS), considering nano-confinement effects, and the initial occurrence state was quantitatively evaluated by combining two-dimensional nuclear magnetic resonance (NMR) and molecular dynamics simulation. The movable fluid saturation was quantitatively determined by centrifugal experiments. The results show that the condensate gas state was in small pores, while the volatile oil state was in large pores. The occurrence states of oil were mainly adsorbed oil and free oil. The proportion of adsorbed oil in inorganic pores was about 24.4%, while the proportion of adsorbed oil in organic pores was about 57.8%. Based on the cutoff value of  $T_2$  before and after the centrifuged laboratory experiments, the movable limit of oil was determined to be 4.5 nm, and the movable fluid saturation was about 11%. The research method proposed in this study has important guiding significance for the initial occurrence state and movability evaluation of similar liquid-rich shale reservoirs.

**Keywords:** Gulong shale oil reservoir; nano-confinement effects; phase behavior; initial occurrence state; movability evaluation



**Citation:** Zhao, G.; Cheng, L.; Jia, P.; Liu, Y.; Feng, H.; Kuang, T.; Wang, Q. Initial Occurrence State and Movability Evaluation of the Gulong Shale Oil Reservoir, Songliao Basin.

*Energies* **2024**, *17*, 1358. <https://doi.org/10.3390/en17061358>

Academic Editor: Reza Rezaee

Received: 9 August 2023

Revised: 14 January 2024

Accepted: 16 January 2024

Published: 12 March 2024



**Copyright:** © 2024 by the authors. Licensee MDPI, Basel, Switzerland. This article is an open access article distributed under the terms and conditions of the Creative Commons Attribution (CC BY) license (<https://creativecommons.org/licenses/by/4.0/>).

## 1. Introduction

The initial occurrence state and movability of fluid, which are closely related to the interaction between the fluid composition and pore throat characteristics, directly determine the development method of a shale oil reservoir [1–4]. However, the pore throat of a shale oil reservoir is mainly nanometer scale. The phase state, physical properties, and flow characteristics of the fluid in the nano space are obviously different from those in the bulk space, which is called nano-confinement effects [5–8]. Therefore, it is challenging to determine the initial occurrence state and movability of fluid in shale nanopores.

In recent years, some scholars have studied the initial occurrence state and movability of fluids through laboratory experiments, empirical methods, etc. Generally speaking, shale oil reservoirs have four initial occurrence states: the free state, adsorption state, swelling state, and dissolution state [9–12]. During an experiment, O’Brien et al. [13] observed that there were two types of occurrence states of liquid oil: one is spherical

oil droplets presented in microfractures, and the other is a coated oil layer present in the microfracture wall. Zhang and Ke [14,15] suggest that there are three kinds of shale oil occurrence states in the reservoir of the Biyang Depression, which are the free state, adsorption state, and dissolution state. Through further research on the location of different occurrence states, it has been found that free oil is presented as oil droplets in nanopores, such as matrix pores, structural fractures, and microfractures of clay, feldspar, dolomite, and other minerals. For adsorbed shale oil, it is mainly presented as an oil film on the surface of clay particles and kerogen. Moreover, an energy spectrum analysis of shale oil in the Biyang Depression by electron microscopy was carried out to verify the above conclusions. Ning et al. [16] believed that the main occurrence states are the free state and the adsorption state. In a study of shale oil movability, Jarvie's research showed that the lower limit of shale oil is about 100 mg/g, which can be characterized by the ratio of pyrolysis parameter S1 to TOC (total organic carbon). The favorable layers of a shale oil reservoir are also divided by oil/TOC [17]. Sun et al. [18] carried out nuclear magnetic resonance combined with centrifugal experiments on 12 high-maturity shale cores to study the distribution characteristics of movable fluid in the cores. Zhou et al. [19] conducted centrifugal experiments on 12 marine Longmaxi shale cores in Southern China and analyzed the minimum pore throat size of movable fluid distribution. Li et al. proposed a conceptual model for calculating the shale adsorption potential ( $S_p$ ) in the Dongying Depression [20]. This model divides the rock into five types: clay minerals, quartz, carbonate minerals, pyrite, and organic matter. Cao et al. studied the conceptual model of shale adsorption potential ( $S_p$ ) calculation for the Qing-1 layer in the Songliao Basin [21]. Fei et al. [22] carried out porosity and permeability tests on Gulong shale cores and analyzed the fluid occurrence space characteristics and imbibition oil recovery based on nuclear magnetic resonance (NMR). Chao et al. [23] conducted a high-speed centrifugation experiment based on NMR and mercury injection experiments to describe the movability of oil and water in shale and developed a mathematical model to analyze the effect of nanopores and the direction of the capillary on the movability of oil and water. Xin et al. [24] used nuclear magnetic resonance (NMR) technology to classify the  $T_2$  spectra of different shale reservoirs, analyzed the correlation between the  $T_2$  cutoff values and the main peaks of the  $T_2$  spectra of the shale reservoirs, and established a rapid identification and evaluation method for different fluid signals of the reservoirs. Artificial intelligence (AI) techniques assist with enhanced oil recovery processes; moreover, the NMR technique provides a new method of EOR for shale oil reservoirs [25–27]. In general, there have been many studies on the occurrence state and movability of shale oil, but the pore throat is not subdivided into organic pores and inorganic pores in these research processes, and there is less evaluation of the fluid state and movability in shale nanopores.

In this study, the Gulong liquid-rich shale reservoir located in the Songliao Basin, China, was selected as the research object. The initial occurrence state and mobility of fluid in the shale nanopores were determined by phase calculation, molecular simulation, and nuclear magnetic resonance. Moreover, a multi-component fluid model was established in the molecular dynamics simulation, which is the innovation of this study. The research results and methods have important guiding significance for the initial occurrence state and movability evaluation of similar shale oil reservoirs.

## 2. Methodology

Due to the impacts of nano-confinement effects in different shale nanopores, the capillary pressure and van der Waals force of fluid molecules in nanopores have changed significantly in the Gulong shale reservoir, which seriously affects the initial occurrence state and movability of fluid [5,8,22]. In this section, a comprehensive research method, including nano-confined phase behavior analysis, NMR (nuclear magnetic resonance), monitoring, and molecular dynamics simulation, is established.

### 2.1. Nano-Confined Phase State Calculation Method

In this study, the modified Peng–Robinson equation of state (modified PR-EOS) is used for phase state calculation. The expression of PR-EOS is as follows:

$$p = \frac{RT}{V - b_m} - \frac{a_m(T)}{V(V + m_1 b_m) + b_m(V + m_2 b_m)} \quad (1)$$

where  $V$  is the molar volume;  $T$  is temperature in K;  $R$  is the gas constant, 8.314 J/(mol·K);  $a_m$  and  $b_m$  represent the attractive and repulsive terms of the mixture, respectively. The van der Waals mixing rule is used to calculate

$$a_m(T) = \sum_{i=1}^n \sum_{j=1}^n x_i x_j (a_i a_j \alpha_i \alpha_j)^{0.5} (1 - k_{ij}) \quad (2)$$

$$b_m = \sum_{i=1}^n x_i b_i \quad (3)$$

The coefficients of the modified PR-EOS are calculated by the following formula:

$$\begin{cases} a = 0.457235529 \frac{R^2 T_c^2}{P_c^2} \\ b = 0.077796074 \frac{RT_c}{P_c} \\ m_1 = 1 + \sqrt{2} \\ m_2 = 1 - \sqrt{2} \end{cases} \quad (4)$$

$$\alpha = \begin{cases} [1 + (0.37464 + 1.54266\omega_i - 0.26992\omega_i^2)(1 - T_{ri}^{0.5})]^2 & \omega_i \leq 0.49 \\ [1 + (0.379642 + 1.48503\omega_i - 0.164423\omega_i^2 + 0.016666\omega_i^3)(1 - T_{ri}^{0.5})]^2 & \omega_i > 0.49 \end{cases} \quad (5)$$

where  $\omega_i$  is the acentric factor,  $k_{ij}$  is the binary interaction coefficient,  $T_r$  is the reduced temperature; and  $\alpha$  is a dimensionless function of reduced temperature and acentric factor. In order to accurately explain the phase behavior of fluid in nano-confined pores, the nano-confinement effects are considered as critical parameters, proposed by Zarragoicoechea and Kuz [28]. The expression is as follows:

$$\Delta P_c = \frac{P_c - P_{cm}}{P_c} = 0.9409(\sigma_{LJ}/R) - 0.2415(\sigma_{LJ}/R)^2 \quad (6)$$

$$\Delta T_c = \frac{T_c - T_{cm}}{T_c} = 0.9409(\sigma_{LJ}/R) - 0.2415(\sigma_{LJ}/R)^2 \quad (7)$$

where  $\Delta P_c$  and  $\Delta T_c$  are relative critical temperature and pressure shift, respectively (dimensionless).  $P_c$  is the critical pressure in bulk space, atm.  $T_c$  is the bulk critical temperature in bulk space, K.  $P_{cm}$  is the critical pressure in nano-confined space, atm.  $T_{cm}$  is the critical temperature in nano-confined space, K.  $\sigma_{LJ}$  is the Lennard–Jones size parameter, nm.  $R$  is the pore radius, nm. It should be noted that  $P_{cm}$  and  $T_{cm}$  are the modified critical pressure and temperature for the nano-confined space. In Equations (6) and (7), we use these two equations and the  $\sigma_{LJ}$  and  $R$  to calculate  $P_{cm}$  and  $T_{cm}$ . So,  $P_{cm}$  and  $T_{cm}$  are determined using Equations (6) and (7) and the for the next calculation.

In addition, due to the large matrix pore space in conventional reservoirs, the flash calculation model ignores the effects of vapor–liquid capillary pressure. However, in shale nanopores, vapor–liquid capillary pressure will significantly affect the phase equilibrium. The fugacity balance considering capillary pressure is as follows:

$$\mu_{L,i}(P_L, x_i) = \mu_{V,i}(P_V, y_i) \quad (8)$$

where  $\mu_{V,i}$ ,  $\mu_{L,i}$  are the chemical potentials of component  $i$  in the vapor phase and liquid phase, respectively.  $x_i$  and  $y_i$  are the concentrations of liquid and vapor components, respectively.  $P_L$  and  $P_V$  are liquid and vapor pressure, MPa, respectively. The capillary pressure between the vapor and liquid is calculated by the Young–Laplace formula as follows:

$$P_{cap} = P_V - P_L = \frac{2\sigma \cos \theta}{R} \quad (9)$$

where  $P_{cap}$  is capillary pressure, MPa.  $\sigma$  is interfacial tension, mN/m.  $\theta$  is the contact angle, °. In this study, the parachor model is used to estimate the vapor–liquid interfacial tension [9]:

$$\sigma = \sum_i^{N_c} (\rho_L [P]_i x_i - \rho_V [P]_i y_i) \quad (10)$$

where  $\rho_L$  and  $\rho_V$  are the molar densities of the liquid and vapor phases, respectively, mol/m<sup>3</sup>.  $[P]_i$  is the parachor of component  $i$ . When vapor–liquid phases are in equilibrium, the fugacity of gas phase and liquid phase is equal. The liquid–vapor equilibrium calculation is carried out using the successive iteration method, which is shown in Figure 1. Table 1 shows the reconstituted components of crude oil and thermodynamic parameters, which are obtained by experiments.

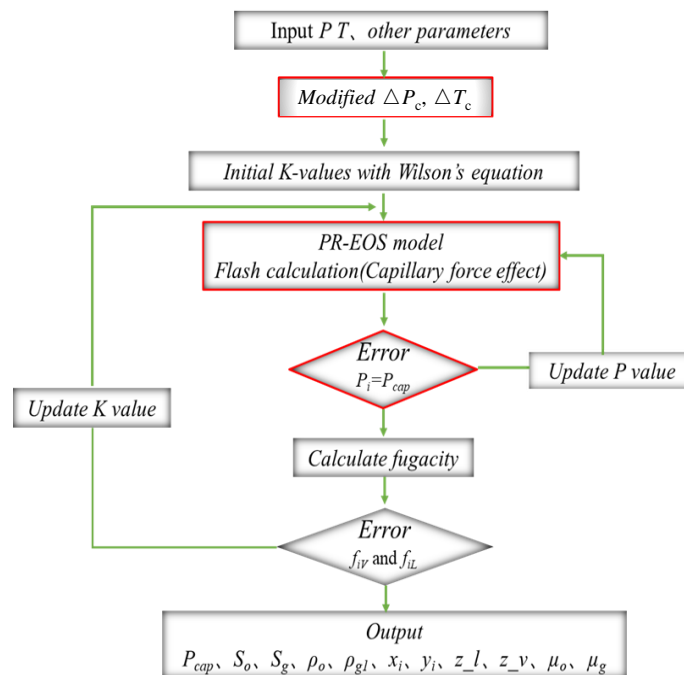


**Figure 1.** Flow chart of liquid–vapor equilibrium calculation considering nano-confinement effects.

**Table 1.** Fluid components and thermodynamic properties.

Components	Mole Fraction, %	Critical Temperature, K	Critical Pressure, MPa	Acentric Factor	Molecular Weight, g/mol	Critical Volume, m <sup>3</sup> /mol	Relative Density
N <sub>2</sub>	1.86	126.20	3.46	0.04	28.01	0.09	0.81
CO <sub>2</sub>	3.98	304.19	7.382	0.23	44.01	0.09	0.82
C <sub>1</sub>	54.84	190.56	4.599	0.01	16.04	0.10	0.30
C <sub>2</sub> –C <sub>5</sub>	23.55	352.09	4.452	0.14	40.07	0.18	0.44
C <sub>6</sub> –C <sub>10</sub>	4.59	582.04	2.805	0.32	111.18	0.43	0.75
C <sub>11</sub> –C <sub>20</sub>	7.90	721.12	1.79	0.54	204.96	0.80	0.83
C <sub>21</sub> –C <sub>30</sub>	2.94	833.44	1.257	0.80	327.19	1.31	0.88
C <sub>31+</sub>	0.32	906.97	0.918	0.92	428.96	1.74	0.92

### 2.2. Nuclear Magnetic Resonance Experimental Method

In this section, we use the NMR methodology to obtain the pore radius of the core from the Q1 and Q3 subzones of the Qing-1 layer of the Gulong shale oil reservoir. The pore radius is a basic and key parameter for the nano-confined phase state calculation and analysis of the initial occurrence state in nanopores. The nuclear magnetic resonance (NMR) monitoring experiment uses the Macro12-150H-I low-field nuclear magnetic resonance (LF-NMR) instrument (Niumag Analytical Instrument Corporation, Suzhou, China), and the centrifugal test uses CSC-12S super-core high-speed freezing centrifuge (Lu Xiangyi Centrifuge Instrument Co., Ltd., Shanghai, China). The cores of the experiment are the actual core from the Q1 and Q3 subzones of the Qing-1 layer of the Gulong shale oil reservoir. The principle of LF-NMR monitoring is based on the relaxation characteristics of the hydrogen nucleus in the fluid when it is affected by the external magnetic field. The nuclear magnetic resonance signals of different pore sizes are analyzed using the mathematical explanation method. The expression is as follows:

$$M(t) = M_0 e^{-\frac{t}{T_2}} = M_0 e^{-\frac{2n\tau}{T_2}} \tag{11}$$

where  $M(t)$  is the echo amplitude at time  $t$ .  $2\tau$  is the echo interval.  $M_0$  is the initial echo amplitude.  $n$  is the number of echoes. The relaxation time  $T_2$  mainly includes the bulk relaxation time, surface relaxation time, and diffusion relaxation time. The expression is as follows:

$$\frac{1}{T_2} = \frac{1}{T_{2S}} + \frac{1}{T_{2B}} + \frac{1}{T_{2D}} = \rho_2 \frac{S}{V} + \frac{1}{T_{2B}} + \frac{D_f(\gamma GT_E)^2}{12} \tag{12}$$

where  $T_{2S}$  is the surface relaxation time, ms.  $T_{2B}$  is the bulk relaxation time, ms.  $T_{2D}$  is the diffusion relaxation time, ms.  $\rho_2$  is the surface relaxation strength,  $\mu\text{m}/\text{ms}$ .  $S/V$  is the area-volume ratio,  $1/\mu\text{m}^2$ .  $D_f$  is the bulk diffusion coefficient of fluid,  $\mu\text{m}^2/\text{ms}$ .  $\gamma$  is the gyromagnetic ratio,  $\text{MHz}/\text{T}$ .  $G$  is the magnetic field gradient,  $\text{G}/\mu\text{m}$ .  $T_E$  is the echo interval, ms, where the bulk relaxation time and diffusion relaxation time can be neglected; then, Equation (12) can be simplified as

$$\frac{1}{T_2} = \frac{1}{T_{2S}} = \rho_2 \frac{S}{V} \tag{13}$$

The area-volume ratio  $S/V$  can be written as a function of the geometric shape factor and the pore radius. Moreover, considering that the geometric shape factor and the surface relaxation strength are constant for a certain porous medium, the conversion relationship between  $T_2$  and the pore radius  $r$  can be obtained. The expression is as follows:

$$T_2 = \frac{1}{\rho_2} \frac{V}{S} = \frac{r}{\rho_2 F_S} = \frac{r}{C} \tag{14}$$

where  $r$  is the pore radius,  $\mu\text{m}$ .  $F_S$  is the geometry shape factor.  $C$  is the conversion coefficient,  $\mu\text{m}/\text{ms}$ . The pore distribution and  $T_2$  spectrum obtained by LF-NMR were calculated using the correlation coefficient method, and the conversion coefficient  $C$  was obtained. The formula is as follows:

$$R = \frac{\sum_{i=1}^n (x_i - \bar{x})(y_i - \bar{y})}{\sqrt{\sum_{i=1}^n (x_i - \bar{x})^2 \sum_{i=1}^n (y_i - \bar{y})^2}} \tag{15}$$

where  $R$  is the correlation coefficient.  $x_i$  is the distribution frequency of the NMR  $T_2$  spectrum in the  $i$  interval, %.  $y_i$  is the pore throat distribution frequency under a scanning electron microscope in the  $i$  interval, %.  $\bar{x}$  is the average frequency of the NMR  $T_2$  spectrum distribution, %.  $\bar{y}$  is the average value of the scanning electron microscope (SEM) distribu-

tion frequency, %. The centrifugal experiment and nuclear magnetic monitoring steps are as follows:

- (1) Measure the dry weight of the core by balance and test  $T_2$  spectrum of dry rock samples with a nuclear magnetic resonance instrument.
- (2) Saturate the shale core with oil samples, and maintain the saturation process for 15 days. Measure the quality of the shale core after saturation; obtain the NMR  $T_2$  spectrum and 2D  $T_1$ - $T_2$  spectrum of shale rock samples after saturation.
- (3) Centrifuge the saturated shale core at 2000 r/min, 6000 r/min, and 10,000 r/min (the maximum speed of the instrument), measure the weight, and obtain the NMR  $T_2$  spectrum after centrifugation.

### 2.3. Molecular Simulation Method

The study of molecular simulation in this study is mainly divided into three steps. The first step is to construct the basic model and the geometric structure. The second step is to use the basic model and geometric structure optimization to calculate the mineral and fluid model. The third step is to use the Forcite module of Materials Studio 2020 software for molecular dynamics simulation and analyze the area where the adsorption phase is located based on the adsorption density distribution curve.

The purpose of geometric optimization is to find the most stable structure of the molecule. The method is to use the optimal force field and algorithm to calculate the potential energy of the whole system and find the structure with the lowest potential energy in the system. The potential energy in the system can be expressed as the sum of valence energy  $E_{\text{valence}}$ , crossterm energy  $E_{\text{crossterm}}$ , and non-bond interaction  $E_{\text{non-bond}}$ .

$$E_{\text{total}} = E_{\text{valence}} + E_{\text{crossterm}} + E_{\text{non-bond}} \quad (16)$$

The universal force field (UFF) and the charge equilibrium (Qeq) method are used to calculate the force field of the mineral model and fluid model. The steepest descent iterative algorithm is used to optimize the first 1000 steps, and then the Smart algorithm is used to calculate the optimal structure of 2000 steps. In the iterative process, the convergence threshold of energy is  $1 \times 10^{-4}$  kcal/mol, the convergence threshold of the external force is  $5 \times 10^{-2}$  kcal/mol/nm, the convergence threshold of internal stress is  $5 \times 10^{-3}$  Gpa, and the convergence threshold of displacement is  $5 \times 10^{-6}$  nm. In order to calculate the electrostatic potential energy, the Ewald summation method is used, and the accuracy is  $1 \times 10^{-4}$  kcal/mol. The atom-based algorithm is used to calculate the van der Waals force between molecules, and a truncation radius of 1.55 nm is used.

The Lennard–Jones potential energy model is used to calculate the interaction between van der Waals force and electrostatic force. The calculation formula is:

$$E = \varepsilon_{ij} \left[ \left( \frac{\delta_{ij}}{r_{ij}} \right)^{12} - \left( \frac{\delta_{ij}}{r_{ij}} \right)^6 \right] + \frac{q_i q_j}{4\pi\epsilon_0 r_{ij}} \quad (17)$$

$$\begin{cases} \delta_{ij} = \frac{\delta_i + \delta_j}{2} \\ \varepsilon_{ij} = \sqrt{\varepsilon_i \varepsilon_j} \end{cases} \quad (18)$$

where  $r_{ij}$  is the distance between the molecule or atom  $i$  and  $j$ , nm.  $\epsilon_0$  is the dielectric constant,  $8.854 \times 10^{-12}$  F/m.  $\varepsilon_{ij}$  is L-J potential energy parameters, kJ/mol.  $\delta_{ij}$  is the collision diameter of atoms, nm.

The biggest difference between shale oil reservoirs and conventional reservoirs is the in situ reservoir formation. Therefore, in addition to inorganic pores, there are also a large number of organic pores (kerogen) in Gulong shale oil reservoirs. In this study, the inorganic pore model and organic pore model are established based on the mineral distribution of the Qing-1 layer of the Gulong shale oil reservoir, and the fluid model

of oil is established based on the fluid components in Table 1. The models are shown in Figures 2 and 3.

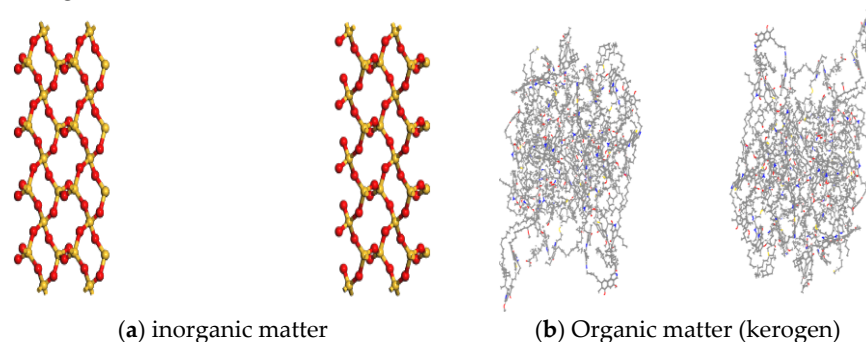


**Figure 2.** Diagram of rock skeleton model in Gulong shale oil reservoir.

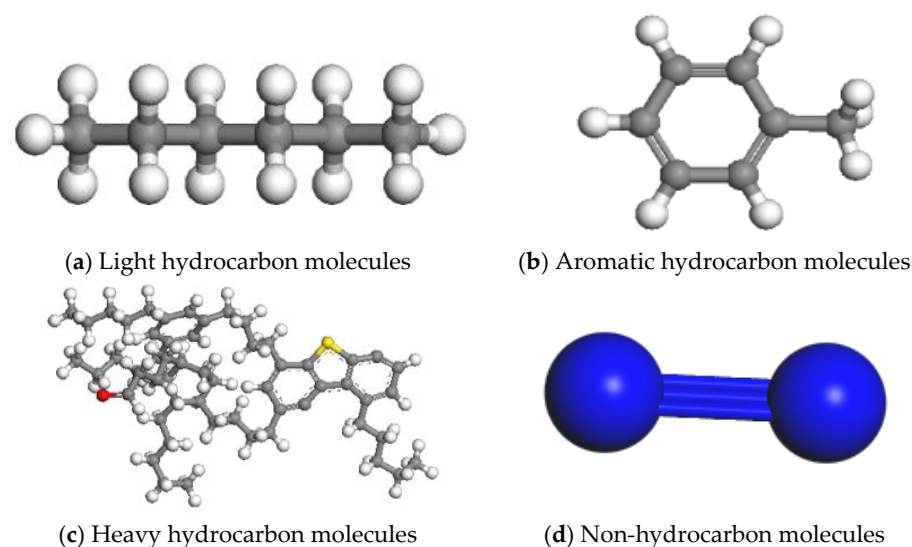


**Figure 3.** Diagram of fluid model in Gulong shale oil reservoir.

### 3. Results and Analysis

#### 3.1. Phase Behavior in Shale Nanopores

Figure 4 shows the phase envelope of fluid in nanopores (radius: 3 nm, 5 nm, 10 nm, 20 nm) and bulk space. The phase state of fluid in the bulk space can be considered as that in bedding fractures and hydraulic fractures. Under the impact of the nano-confinement effect, the bubble point line and dew point line of the fluid shrink inward, and the area of the two-phase coexistence zone of the fluid is significantly reduced. Moreover, the smaller the pore size, the greater the decrease in the saturation pressure of the hydrocarbon fluid.

For conventional oil reservoirs, the relative position of the initial formation pressure and temperature of the reservoir in the phase diagram are used to determine whether the reservoir type is a black oil reservoir, volatile oil reservoir, condensate gas reservoir, or dry gas reservoir. However, in the shale nanopores, the fluid in different pore sizes shows different phase behaviors, and the heterogeneity of the pore structure distribution aggravates the difference in the phase state in different pores. In this study, the shale nanopores are considered as a ‘supply source’. The phase behavior of the ‘supply source’ is affected by the pore radius. Then, the shale reservoir with a complex pore distribution structure is divided into multiple types of ‘supply sources’ with several phase behavior characteristics. As shown in Figure 5, the black solid line and the imaginary line are the phase envelope curves under weak nano-confinement (50 nm pore radius) and strong nano-confinement (3 nm pore radius), respectively. I–IV are the relative positions of the initial temperature and pressure conditions in the phase diagram. When the initial temperature and pressure of the reservoir are in the relative position I, the hydrocarbon fluid in the pores

with weak nano-confinement (50 nm) presents a black oil state, while the hydrocarbon fluid in the pores with strong nano-confinement (3 nm) presents volatile oil state, and the nanopores of this reservoir are the ‘supply source’ of black oil–volatile oil. When the initial temperature and pressure of the reservoir are in the relative position III, the hydrocarbon fluid in the weak nano-confinement (50 nm) pores presents an oil–gas two-phase state, while the hydrocarbon fluid in the strong nano-confinement (3 nm) pores presents a dry/wet gas state; thus, the nanopores in this reservoir are the ‘supply source’ of volatile oil–dry/wet gas. When the initial temperature and pressure of the reservoir are in the relative position IV, the hydrocarbon fluid in the pores with weak nano-confinement (50 nm) presents condensate gas state, and in the pores with strong nano-confinement (3 nm) presents a dry/wet gas state; thus, the nanopores in this reservoir are the ‘supply source’ of condensate gas–dry/wet gas. The initial temperature and pressure conditions of the Gulong shale reservoir are located at position II, so the nanopores of the Gulong shale oil reservoir are the ‘supply source’ of volatile oil–condensate gas.

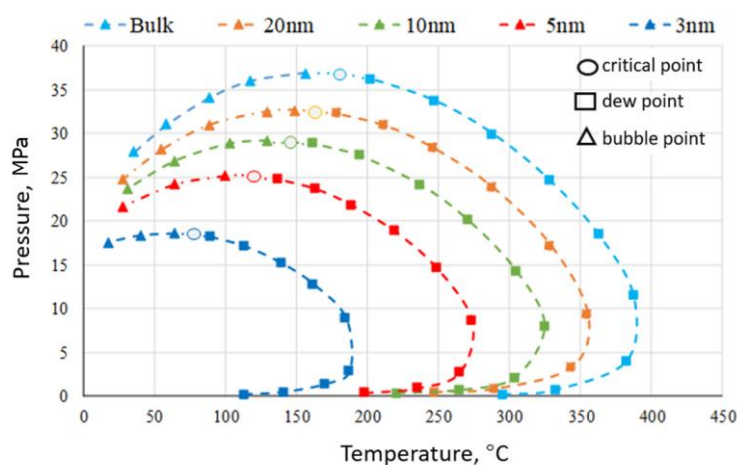


Figure 4. Fluid-phase envelopes in different size of shale nanopores.

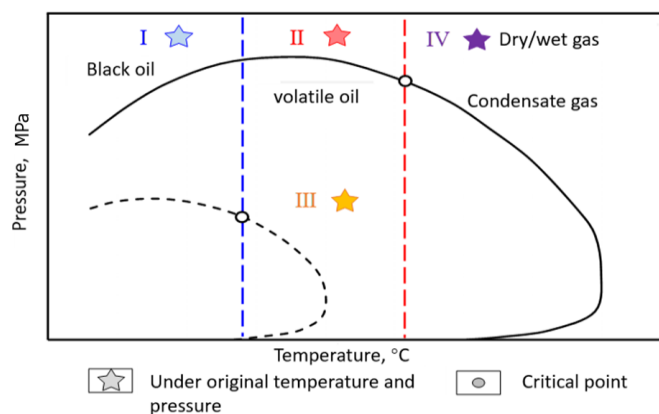


Figure 5. The initial phase state under different initial temperature and pressure conditions.

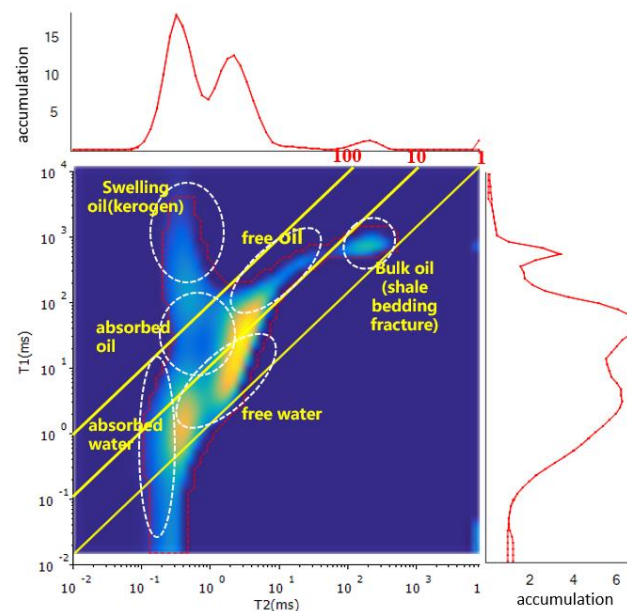
The effective development of the Gulong shale oil reservoir requires the use of a horizontal well and stimulated reservoir volume technology, so that the multi-scale flow space of nano-matrix–microfractures–hydraulic fractures can be created. So, during the stage of fracturing and shut-in, there are differences in the initial occurrence state of fluid in different pores, as shown in Table 2.

**Table 2.** Fluid distribution and phase state in different scale flow spaces.

Type of Porous Media	Range of Pore Radius	Fluid Distribution	Phase State
Nanopores	2–50 nm	Hydrocarbon	Condensate gas state
Shale bedding fracture	100 nm–5000 nm	Hydrocarbon, a small amount of fracturing fluid	Volatile oil state
Hydraulic fracture	>1 mm	Fracturing fluid, a small amount of hydrocarbon	Black oil state

### 3.2. Analysis of Initial Occurrence State

There are four initial occurrence states of shale oil, which include the adsorption state, free state, swelling state, and dissolved state. However, the water cut of the shale oil reservoir is low, and the solubility of crude oil in water is low, so the content of dissolved shale oil can be ignored. In the two-dimensional NMR monitoring of shale, the  $T_1$  value of organic matter (such as kerogen and crude oil) is relatively high, while the  $T_1$  value of water is relatively low. In addition, the  $T_2$  value of the fluid is related to its viscosity and flow capability. The larger the  $T_2$  value, the lower the viscosity of the fluid and the better the flow capability. Therefore, the  $T_1/T_2$  value of organic matter with high viscosity and dense structure such as kerogen is higher, while the  $T_1/T_2$  value of light hydrocarbon with low viscosity and good flow capability is lower. Of course, the signal intensity distribution of different types and maturity of organic matter in each interval will also be different. At present, experts and scholars at home and abroad judge the initial occurrence state of the shale reservoir via the two-dimensional nuclear magnetic  $T_1$ - $T_2$  spectrum, mainly relying on the range of the  $T_2$  boundary value and  $T_1/T_2$  value for interval division. It is generally believed that the distribution interval  $T_1/T_2$  of the water signal is about 1, the distribution interval  $T_1/T_2$  of kerogen is greater than 100, the distribution interval of light hydrocarbon is mainly  $T_1/T_2$  greater than 10, and the  $T_2$  value is about 1. Based on this principle, the initial occurrence state of the Gulong shale reservoir is qualitatively analyzed, including kerogen, adsorbed oil, free oil, bulk oil (oil in fractures), and some initial adsorbed water and free water, which is shown in Figure 6.

**Figure 6.** Two-dimensional  $T_1$ - $T_2$  spectrum and initial occurrence state of Gulong shale oil.

In order to further clarify the occurrence state of hydrocarbon fluids in inorganic pores and organic pores, the relative density functions of fluids in different types of pores are calculated through molecular simulation. Figure 7a,b show the fluid distribution and relative density curves in inorganic pores and organic pores with a pore diameter of 5 nm, respectively. The occurrence state of fluid is comprehensively judged according to the

relative density of skeleton molecules and the relative density of fluid molecules. The hydrocarbon fluids in the inorganic pores are mainly free and adsorbed states, while the hydrocarbon fluids in the organic matter have some swelling crude oil in addition to free and adsorbed states. The swelling crude oil is mainly caused by the dissolution of a part of crude oil by kerogen, which leads to its own volume expansion. The dissolved part of crude oil is called swelling crude oil. However, the content of swelling crude oil is usually low, so the main initial occurrence state of fluid in the nanopores of the Gulong shale oil reservoir is the free state and adsorbed state. For bedding fractures and hydraulic fractures, the main occurrence state is the free state.

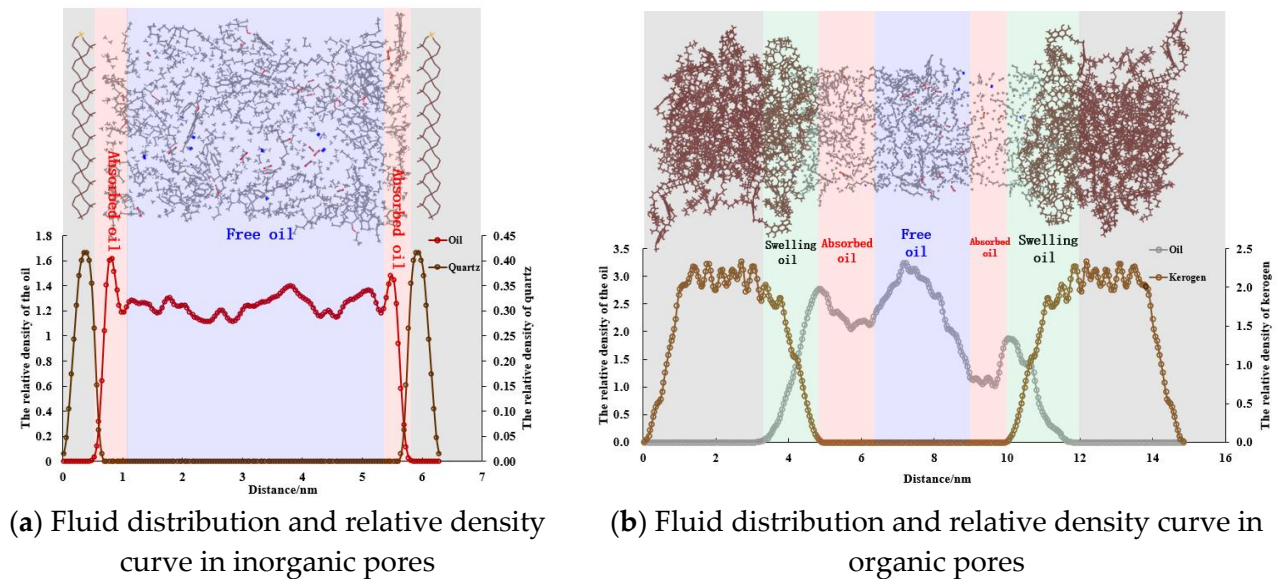


**Figure 7.** Initial occurrence state of fluid in inorganic and organic pores.

### 3.3. Analysis of Adsorbed Oil and Free Oil

Under the conditions of an original formation pressure of 37 MPa and original formation temperature of 135 °C, a molecular simulation scheme of different pore types for the initial occurrence state of fluid molecules in nanochannels is formed, and the distribution of crude oil molecules in different nano-matrix channels is quantitatively characterized. Figure 8a,b show the proportion of free oil and adsorbed oil in 10 nm inorganic and organic pores. In the 10 nm organic pores, the proportion of free oil is 61%, while the proportion of adsorbed oil is 39%. In 10 nm inorganic pores, free oil accounts for 96.3%, while inorganic pores account for 73%. This shows that in the original state, the amount of adsorbed oil in organic pores is larger, and the movable oil is mainly distributed in inorganic pores.

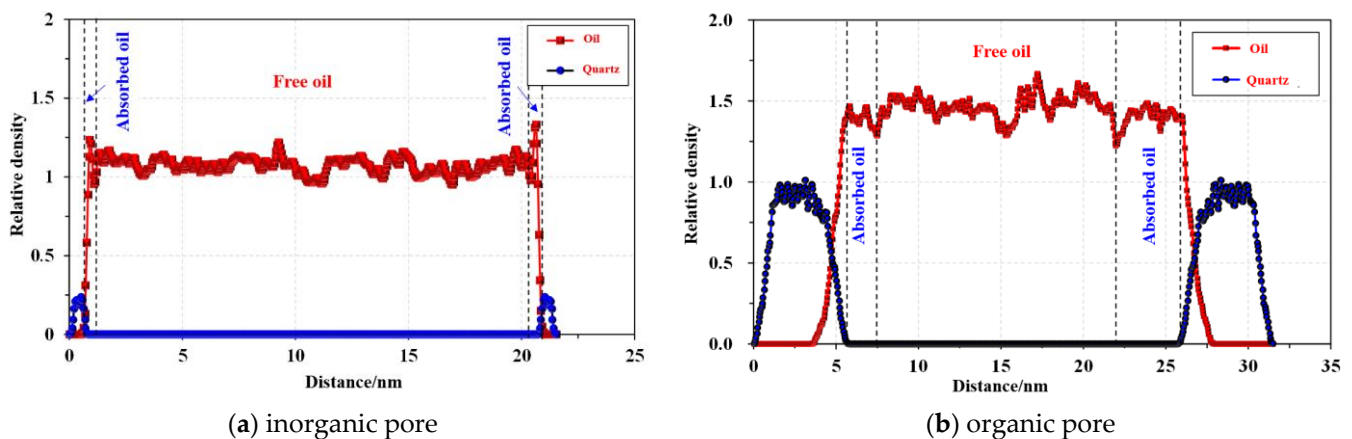


**Figure 8.** The proportion of free oil and adsorption oil in inorganic and organic pores.

By calculating the proportion of free oil and adsorbed oil in a pore radius of 1~30 nm, combined with the mineral content data of Gulong shale oil, it can be calculated that the average volume ratio of adsorbed oil in the inorganic minerals of the Gulong shale reservoir is 24.4%, and the proportion of adsorbed oil in organic pores is about 57.8%.

### 3.4. Analysis of Movable Fluid Saturation

Two cores from the Q1 and Q3 subzones of the GY-10HC well are selected to carry out centrifugal-NMR monitoring experiments at three points with different rotation speeds. The length and diameter of the cores are measured by vernier calipers, and the mass of the cores before and after centrifugation is measured by balance, as shown in Figure 9a,b.

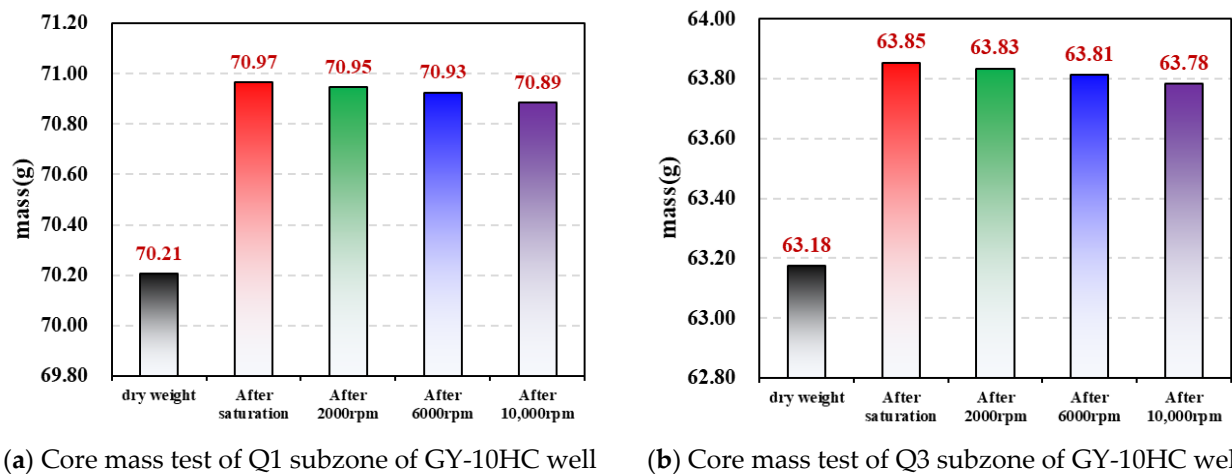


Figure 9. Core mass test results before and after centrifugation.

Figure 10a,b show the  $T_2$  spectrum distribution curves and cumulative distribution curves of the two cores before and after centrifugation. Aiming at the limit of movable porosity of Gulong shale, the  $T_2$  cutoff value and movable porosity of Q1 and Q3 subzones of the GY-10HC well are calculated based on the cumulative distribution curve of the  $T_2$  spectrum before and after centrifugation. The  $T_2$  cutoff value of the core in the Q1 subzone is 2.009 ms, and the movable porosity is 0.471%. The  $T_2$  cutoff value of the core in the Q3 subzone is 3.511 ms, and the movable porosity is about 0.46%. The movable pore throat limit of conventional reservoirs is usually based on the  $T_2$  cutoff value as the standard, but the error of judging the movable limit according to the  $T_2$  cutoff value is large. In this study, the difference in  $T_2$  equaling 1 is proposed as the movable boundary. After comparison, the minimum movable  $T_2$  spectrum of the Gulong shale oil reservoir is about 0.0201~0.0266 ms. Therefore, the movable limit of the pore throat in the Gulong shale reservoir is that the pore throat radius is greater than 4.5 nm, and the movable porosity accounts for about 11% of the total porosity.

For the calculation method of movable fluid saturation, there are mainly the following three categories: ①  $T_2$  Cutoff value method—movable fluid saturation  $S_1$ : the ratio of peak area before cutoff value (movable fluid) and total peak area (total fluid). ② Area method—movable fluid saturation  $S_2$ : using the NMR results after centrifugation, the ratio of the peak area after centrifugation to the peak area after saturation. ③ Mass method—movable fluid saturation  $S_3$ : using the weighing results before and after centrifugation, the mass of the centrifuged core and the saturated core mass. In this study, the average value of the calculated results of the latter two methods is taken as the movable fluid saturation. The calculation results are shown in Table 3. Finally, the movable fluid saturation of the Gulong shale oil reservoir is about 12%.

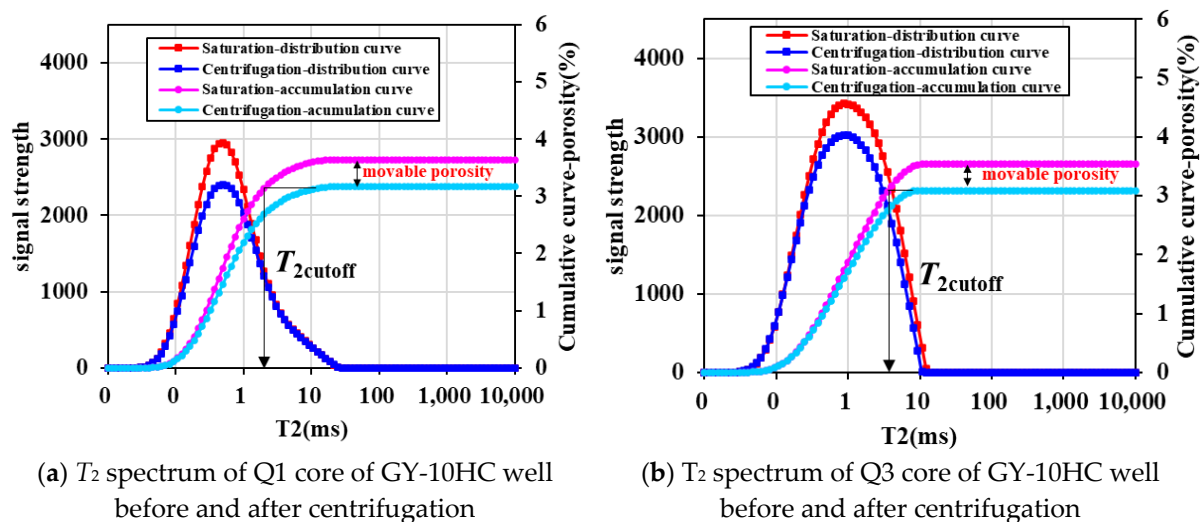


Figure 10. Core NMR test results before and after centrifugation.

Table 3. Movable fluid saturation of GY-10HC in Gulong shale oil reservoir.

Well Name	Subzone	$T_2$ Cutoff Value Method—S1	$T_2$ Area Method—S2	Mass of Cores Method—S3	Movable Fluid Saturation S
GY-10HC	Q1	15.87%	12.95%	10.51%	11.73%
	Q3	16.34%	12.72%	10.32%	11.52%

#### 4. Conclusions

This study focuses on the initial occurrence state and movability of the Gulong shale reservoir fluid in the Songliao Basin, and a comprehensive research method, including nano-confined phase state analysis, nuclear magnetic resonance monitoring, and molecular simulation, is established. The following conclusions are obtained:

- (1) Considering the nano-confinement effects, the nanopores of the Gulong shale reservoir present the characteristics of a ‘condensate gas state in small pores and volatile oil state in large pore’.
- (2) The initial occurrence state of the Gulong shale reservoir is mainly the adsorbed state and free state. The adsorbed oil in inorganic pores accounts for about 24.4%, and the adsorbed oil in organic pores accounts for about 57.8%.
- (3) The minimum movable limit of the pore throat in the Gulong shale reservoir is determined by centrifugation and the nuclear magnetic resonance method. The movable porosity accounts for about 11% of the total porosity, and the movable fluid saturation is about 12%.

**Author Contributions:** Conceptualization, G.Z. and L.C.; methodology, G.Z.; software, P.J.; validation, Y.L. and H.F.; formal analysis, L.C.; investigation, P.J. and Y.L.; data curation, T.K. and Q.W.; writing—original draft preparation, H.F. and T.K.; writing—review and editing, P.J.; supervision, G.Z.; project administration, L.C.; funding acquisition, G.Z. All authors have read and agreed to the published version of the manuscript.

**Funding:** This research was funded by the CNPC Major Technology Project “Theory and Key Technologies of Exploration and Development of Daqing Gulong Shale Oil”, Topic 2 “Theory and Key Technologies of Beneficial Development of Gulong Shale Oil”, grant number 2021ZZ10-02.

**Data Availability Statement:** Data are contained within the article.

**Conflicts of Interest:** Authors Guozhong Zhao, Yong Liu, Tie Kuang and Qingzhen Wang were employed by the Exploration and Development Research Institute of Daqing Oilfield Company Ltd. The remaining authors declare that the research was conducted in the absence of any commercial or financial relationships that could be construed as a potential conflict of interest.

## References

1. Lu, S.; Huang, W.; Chen, F.; Li, J.; Wang, M.; Xue, H.; Wang, W.; Cai, X. Classification and evaluation criteria of shale oil and gas resources: Discussion and application. *Pet. Explor. Dev.* **2012**, *39*, 268–276. [[CrossRef](#)]
2. Sun, L.; Liu, H.; He, W.; Li, G.; Zhang, S.; Zhu, R.; Jin, X.; Meng, S.; Jiang, H. An analysis of major scientific problems and research paths of Gulong shale oil in Daqing Oilfield, NE China. *Pet. Explor. Dev.* **2021**, *48*, 527–540. [[CrossRef](#)]
3. Wang, Y.; Liang, J.; Zhang, J.; Zhao, B.; Zhao, Y.; Liu, X.; Xia, D. Resource potential and exploration direction of Gulong shale oil in Songliao Basin. *Pet. Geol. Oilfield Dev. Daqing* **2020**, *39*, 20–34.
4. Zou, C.; Yang, Z.; Cui, J.; Zhu, R.; Hou, L.; Tao, S.; Yuan, X.; Wu, S.; Lin, S.; Wang, L.; et al. Formation mechanism, geological characteristics and development strategy of nonmarine shale oil in China. *Pet. Explor. Dev.* **2013**, *40*, 15–27. [[CrossRef](#)]
5. He, W.; Meng, Q.; Feng, Z.; Zhang, J.; Wang, R. In-situ accumulation theory and exploration & development practice of Gulong shale oil in Songliao Basin. *Shiyou Xuebao/Acta Pet. Sin.* **2022**, *43*, 1–14. [[CrossRef](#)]
6. Jiang, Z.; Zhang, W.; Liang, C.; Wang, Y.; Liu, H.; Chen, X. Characteristics and evaluation elements of shale oil reservoir. *Shiyou Xuebao/Acta Pet. Sin.* **2014**, *35*, 184–196. [[CrossRef](#)]
7. Liu, H.; Zhang, S.; Bao, Y.; Fang, Z.; Yao, S.; Wang, Y. Geological characteristics and effectiveness of the shale oil reservoir in Dongying sag. *Oil Gas Geol.* **2019**, *40*, 512–523. [[CrossRef](#)]
8. Wang, F.; Fu, Z.; Wang, J.; Tang, Z.; Jiang, R. Characteristics and classification evaluation of Gulong shale oil reservoir in Songliao Basin. *Pet. Geol. Oilfield Dev. Daqing* **2021**, *40*, 144–156.
9. Tian, S. Microscopic Characteristics of Shale Reservoir Pores and Evaluation of Shale Oil Occurrence and Mobility. Ph.D. Thesis, China University of Petroleum (East China), Qingdao, China, 2019.
10. Zhang, X. Research on New Methods for Characterizing Pore Structure of Shale Oil and Gas Reservoirs. Master's Thesis, University of Chinese Academy of Sciences (Institute of Seepage Fluid Mechanics, Chinese Academy of Sciences), Beijing, China, 2021.
11. Li, J. Study on the Occurrence Mechanism and Mobility of Shale Oil. Ph.D. Thesis, China University of Petroleum (East China), Qingdao, China, 2020.
12. Lu, S.; Chen, F.; Xiao, H.; Li, J.; He, X. Quantitative evaluation of organic and inorganic pores in shale reservoirs—Taking the Lower Cambrian Niutitang Formation in Qiannan Depression as an example. In Proceedings of the 14th Annual Conference of the Chinese Society of Mineral and Rock Geochemistry, Nanjing, China, 21 April 2013; p. 1.
13. O'Brien, N.R.; Cremer, M.D.; Canales, D.G. The Role of Argillaceous Rock Fabric in Primary Migration of Oil. *GCAGS Trans.* **2002**, *52*, 1103–1112.
14. Zhang, W. Characteristics and evaluation factors of shale oil reservoirs in the third member of Paleogene Hetaoyuan Formation in Biyang Sag. Master's Thesis, China University of Geosciences (Beijing), Beijing, China, 2014.
15. Ke, S. Discussion on occurrence state and mobility of shale oil in Biyang sag. *Pet. Geol. Eng.* **2017**, *31*, 80–83.
16. Ning, F.; Wang, X.; Hao, X.; Jiang, X.; Wang, Y.; Zhu, D.; Zhu, D. Study on evaluation method of shale oil sweet spot in Jiyang depression. *Sci. Technol. Eng.* **2015**, *35*, 11–16.
17. Jarvie, D. Shale resource systems for oil and gas: Part 2: Shale-oil resource systems. *AAPG Mem.* **2012**, *97*, 89–119.
18. Sun, J.; Chen, J.; Yang, Z.; Liu, X.; Liu, Y. Experimental Study of the NMR Characteristics of Shale Reservoir Rock. *Sci. Technol. Rev.* **2012**, *30*, 25–30.
19. Zhou, S.; Liu, H.; Yan, G.; Xue, H.; Guo, W. NMR research of movable fluid and T<sub>2</sub> cutoff of marine shale in South China. *Oil Gas Geol.* **2016**, *37*, 612–616.
20. Li, Z.; Zou, Y.-R.; Xu, X.-Y.; Sun, J.-N.; Li, M.; Peng, P.A. Adsorption of mudstone source rock for shale oil—Experiments, model and a case study. *Org. Geochem.* **2016**, *92*, 55–62. [[CrossRef](#)]
21. Cao, H.; Zou, Y.-R.; Lei, Y.; Xi, D.; Wan, X.; Peng, P.A. Shale Oil Assessment for the Songliao Basin, Northeastern China, Using Oil Generation-Sorption Method. *Energy Fuels* **2017**, *31*, 4826–4842. [[CrossRef](#)]
22. Xu, F.; Jiang, H.Q.; Liu, M.; Jiang, S.; Wang, Y.; Li, J.J. NMR-Based Analysis of Fluid Occurrence Space and Imbibition Oil Recovery in Gulong Shale. *Processes* **2023**, *11*, 1678. [[CrossRef](#)]
23. Zhu, C.F.; Guo, W.; Li, Y.J.; Gong, H.J.; Sheng, J.J.; Dong, M.Z. Effect of occurrence states of fluid and pore structures on shale oil movability. *Fuel* **2021**, *288*, 119847. [[CrossRef](#)]
24. Sun, X.; Du, H.; Wang, C.; Du, S.; Liu, G. Characterization of Shale Porosity and Permeability by Nuclear Magnetic Resonance. In Proceedings of the 2nd International Conference on Energy Utilization and Automation, ICEUA 2023, Virtual, Online, China, 10–12 February 2023.
25. Zarragoicoechea, G.J.; Kuz, V.A. Critical shift of a confined fluid in a nanopore. *Fluid Phase Equilibria* **2004**, *220*, 7–9. [[CrossRef](#)]
26. Guerillot, D.R. EOR Screening with an Expert System. In Proceedings of the Petroleum Computer Conference, San Jose, CA, USA, 27–29 June 1988; Article No. SPE-17791-MS. [[CrossRef](#)]

27. Alvarado, V.; Manrique, E. Chapter 8: EOR's Current Status. In *Enhanced Oil Recovery*; Alvarado, V., Manrique, E., Eds.; Gulf Professional Publishing: Boston, MA, USA, 2010; pp. 133–156. [[CrossRef](#)]
28. Lyons, W. *Working Guide to Reservoir Engineering*; Gulf Professional Publishing: Houston, TX, USA, 2009.

**Disclaimer/Publisher's Note:** The statements, opinions and data contained in all publications are solely those of the individual author(s) and contributor(s) and not of MDPI and/or the editor(s). MDPI and/or the editor(s) disclaim responsibility for any injury to people or property resulting from any ideas, methods, instructions or products referred to in the content.